Doctoral Forum on Vacuum Electronics (FVE 2017)

22–23 August 2017

Design of W-band sheet beam travelling wave tubes based on staggered double vane slow wave structure

Hanwen Tian[1], Wei Shao[1], Zhanliang Wang[1], Yanyu Wei[1], Zhaoyun Duan[1], Yubin Gong[1], Jinjun Feng[2]

[1]*National Key Laboratory of Science and Technology on Vacuum Electronics, University of Electronic Science and Technology of China, No. 4, Section 2, North Jianshe Road, Chengdu, People's Republic of China*
[2]*Beijing Vacuum Electronics Research Institute, Beijing, People's Republic of China*
E-mail: ybgong@uestc.edu.cn

Published in *The Journal of Engineering*; Received on 8th February 2018; Revised on 2nd March 2018; Accepted on 13th April 2018

Abstract: In this study, a complete and viable plan about a W-band sheet beam travelling wave tube based on a staggered double vane slow wave structure is drawn up. The dispersion characteristics, transposition characteristics of high-frequency system, sheet electron beam gun, vacuum window, periodically cusped magnetic focusing system and beam–wave interaction are analysed by CST Microwave Studio, CST Particle Studio and HFSS. An attenuator is used in this device to suppress oscillation. A phase velocity taper is used to increase output power. The operation voltage is 20.6 kV and the current is 80 mA. With a 10 W input power, the output power is 1100 W versus the gain is 20.41 dB at 95 GHz. The peak amplitude approaches 1200 W versus the gain approaches 20.79 dB at 99 GHz.

1. Introduction

Nowadays, short-millimeter wave devices are increasingly used in high-speed communication, high-resolution imaging and so on [1, 2]. There are some special bands which have little attenuation in the atmosphere at 35, 94, 140, 220 GHz and so on which are called atmosphere windows [3]. Therefore, it is necessary to design a microwave source at 94 GHz (in W-band) [4]. In practice, conventional travelling wave tubes (TWT) which work at a high-frequency band lose a mass of power in the high-frequency structure so that the bandwidth is narrow and dispersion characteristic will change [5–7].

Compared with pencil beam devices, sheet beam devices have more advantages in such a high frequency [8]. While the sheet beam TWT is a kind of important device of sheet beam devices, the staggered double vane slow wave structure (SWS) is an important structure as the core of sheet beam TWTs [9, 10]. The heat dissipation properties of staggered double vane SWS is satisfying because of its all-metal structure and low power loss. The highly efficient energy conversion and high-power capability are also attractive advantages of this structure [5, 11].

However, the staggered double vane SWS needs a sheet electron beam. At the same time, the wave with a high frequency requires small dimensions of device. That means the current of the device is restrictive because the current density could not increase infinitely, which results in the restriction of power. The sheet electron beam is a good method to solve this problem. One dimension of the sheet electron beam is closely related to the operating frequency, while the other dimension rarely affects the operating frequency. Therefore, we could get a larger cross-sectional area by increasing the dimension rarely related to the operating frequency to reduce the space charge force and get a wider interaction area to enhance the output power.

Due to these benefits of the sheet electron beam, it is vital to design an electron gun which could emit sheet electron beam. The TWT in such a high-frequency band always has a significant loss. To keep a satisfying output power, a large emission current is necessary. Thus, the difficulty of the W-band sheet beam electron gun is keeping the balance between the small dimensions and the large emission current.

To focus the sheet electron beam, a periodically cusped magnet (PCM) focusing system is utilised [12].

In section 2, schematic diagrams of high-frequency structure and an attenuator are given, dispersion characteristic of the staggered double vane SWS is analysed and transportation characteristics with and without the attenuator are simulated. A vacuum window is also analysed. In section 3, a sheet beam gun supporting W-band TWT is introduced. A suitable PCM focusing system is designed. In section 4, the interaction between beam and wave is simulated. A phase velocity taper is used to improve the output power. The output power and gain in the frequency range from 90 to 107 GHz are given. In section 5, the whole work of this paper is summarised.

2. Dispersion characteristics and transportation characteristics

2.1 Dimensions and schematic diagrams

As the core of the TWT shown in Fig. 1, the SWS is the place where the wave interacts with the electron beam. Its dimensions are shown in Table 1. To match the electron beam with wave, the dispersion characteristic is analysed. As shown in Fig. 2, we chose the operation voltage as 20.6 kV.

The high-frequency system includes an attenuator, transition structure and periodic structure, as shown in Fig. 3. The attenuator is used to interrupt the propagation of electromagnetic waves, so as to prevent oscillations. The transition structure could ensure that the structure transit smoothly, which could improve the transportation characteristics significantly.

2.2 Transportation characteristics

As shown in Fig. 3, port 1 is the input port, port 2 is the output port, and ports 3 and 4 are the tunnels of the electron beam. The transition structure and the attenuator could prevent oscillation. The *S* parameters without the attenuator are shown in Fig. 4. The

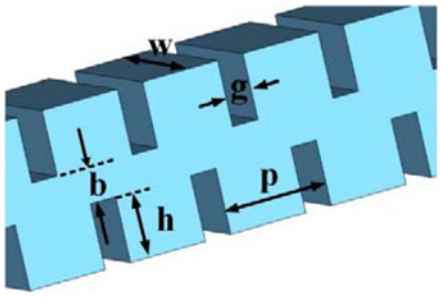

Fig. 1 *Schematic diagram of staggered double vane SWS and dimension parameters*

Table 1 Values of dimension parameters

Parameter	Value, mm
w	1.786
g	0.269
h	0.658
p	1.066
b	0.35

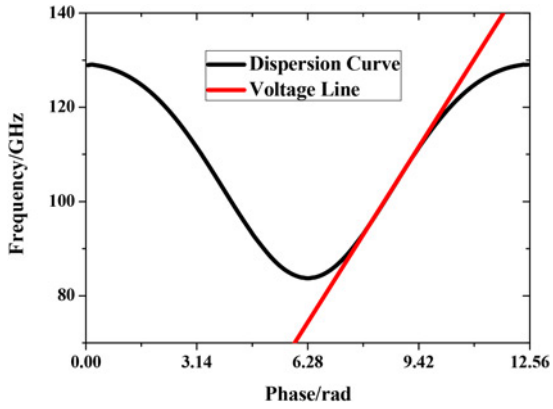

Fig. 2 *Dispersion curve and beam voltage line*

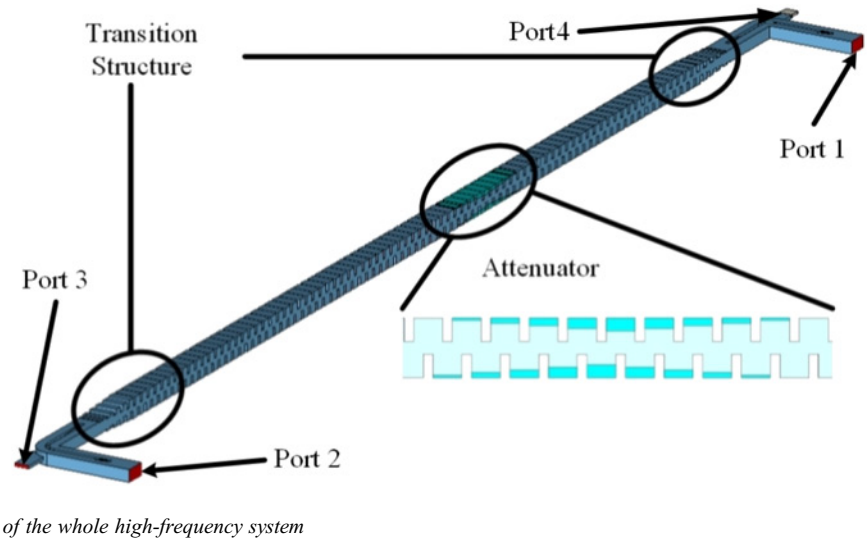

Fig. 3 *Schematic diagram of the whole high-frequency system*

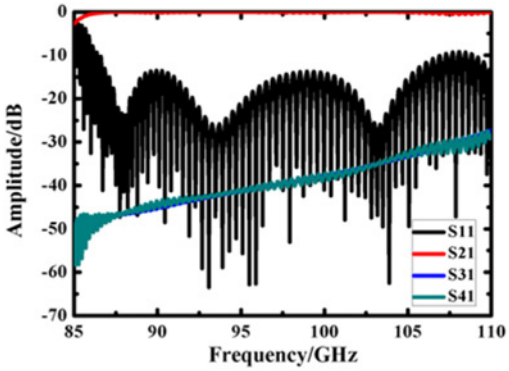

Fig. 4 *S parameters of the high-frequency system without attenuator*

parameter S_{21} is near to 0 dB that means most of the wave passes the structure, while the parameter S_{11} is small that means the reflectance is small. The parameters S_{31} and S_{41} are also very small that means loss in the electron beam tunnels is weak.

The S parameters with the attenuator are shown in Fig. 5 [13]. Compared with Fig. 4, the parameter S_{21} reduced significantly. The parameter S_{11} does not have a clearly change. The parameters S_{31} and S_{41} are still small. Therefore, the attenuator could suppress the oscillation efficiently.

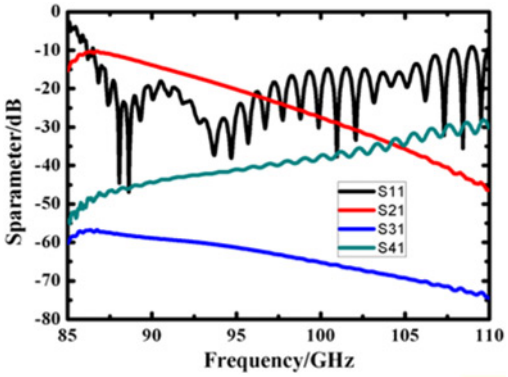

Fig. 5 *S parameters of the high-frequency system with attenuator*

doi: 10.1049/joe.2018.0103

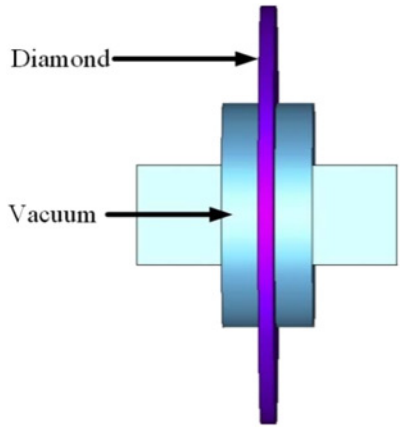

Fig. 6 *Diamond vacuum window*

2.3 Vacuum window

Vacuum window is a very important part of the TWT. Since the input and output signals have to pass through the vacuum window, the transportation characteristic of the vacuum window has a direct effect on the performance of the whole device [14].

As shown in Fig. 6, the material of the vacuum window used in this design is diamond. The rectangular waveguides on the sides of the diamond disk are the standard waveguide of the W-band.

Fig. 7 shows the *S* parameters of the diamond vacuum window. The parameter S_{11} is widely lower than −20 dB from around 91 to around 107 GHz, while the parameter S_{21} is always near to 0 dB. Thus, this diamond vacuum window could meet the design demand.

3. Sheet beam electron gun and PCM focusing system

3.1 Cathode and focusing electrode

A rectangular cathode is chosen to emit the sheet electron beam while a focusing electrode is used to control the shape of the emission sheet electron beam, as shown in Fig. 8 [15].

The emission current density of the cathode could not increase limitlessly. Thus, in order to get a large emission current, we need a large cathode whose dimensions are substantially larger than the electron beam channel. That is why a focusing electrode is necessary.

One of the most important functions of the focusing electrode is compressing the sheet electron beam. The most difficult task is compressing the narrow side of the sheet electron beam. The dimension of the narrow side is closely related to the operating frequency so that there is a large compression ratio in this dimension. A pierce electrode is used here so as to compress the narrow side of the sheet

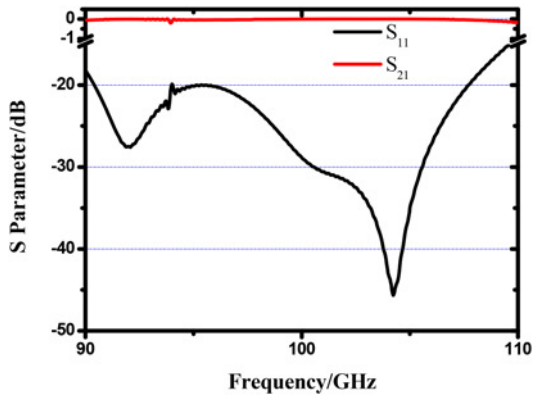

Fig. 7 *Transportation characteristics of the diamond vacuum window*

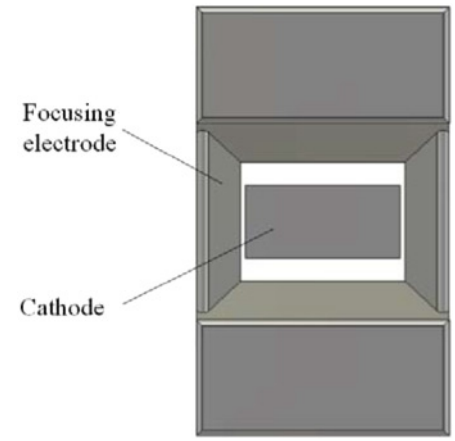

Fig. 8 *Schematic diagram of cathode and focusing electrodes*

electron beam. With theoretical analysis, it will get the best compression effect when the angle between the pierce electrode and *z*-axis is 67.5° [16].

The dimension of the broad side of the sheet electron beam usually does not need such a large compression ratio. Hence, it is not necessary to set the angle between the electrode and *z*-axis to 67.5°. A suitable angle is chosen to compress the broad side of the sheet electron beam. Fig. 9 shows the electrodes of the focusing electrode.

3.2 Anode

The dimensions of the exit of the anode channel are determined by the high-frequency system.

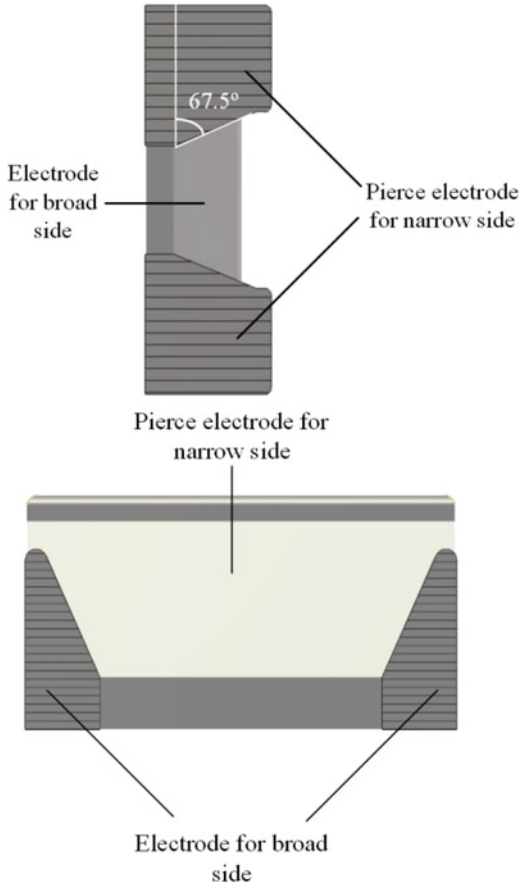

Fig. 9 *Schematic diagram of crossing section of focusing electrode*

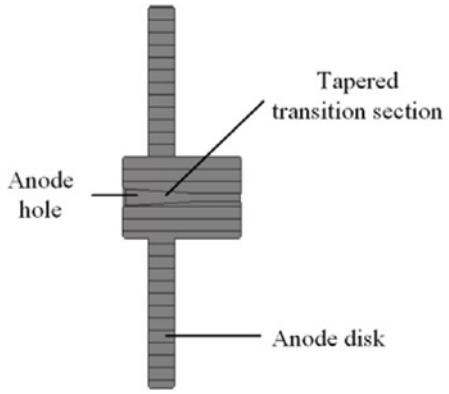

Fig. 10 *Schematic diagram of crossing section of anode*

The dimensions of anode hole are larger than that of the exit of anode channel in order to enhance the propagation rate. A tapered transition section is used to connect the anode hole and the anode channel exit as shown in Fig. 10.

3.3 Shape of the electron beam

According to the design of the high-frequency system, the operation voltage of this sheet electron beam gun is locked at 20.6 kV. The beam current of this electron gun is 0.814 A. Fig. 11 shows the trajectory of the sheet electron beam. The electron beam propagation rate of this sheet beam electron gun is 100%. Fig. 12 shows the cross section of the sheet electron beam at the exit of the anode channel. It indicates that the sheet electron beam emitted by this sheet electron gun could match well with the electron beam channel.

3.4 PCM focusing system

A PCM focusing system is utilised in the design as shown in Fig. 13 [17]. Since the magnetic blocks are arranged periodically along the direction that wave propagates, the z-component magnetic field along the z direction in periodically as shown in Fig. 14. The peak amplitude of the z-component magnetic field approaches 0.467 T.

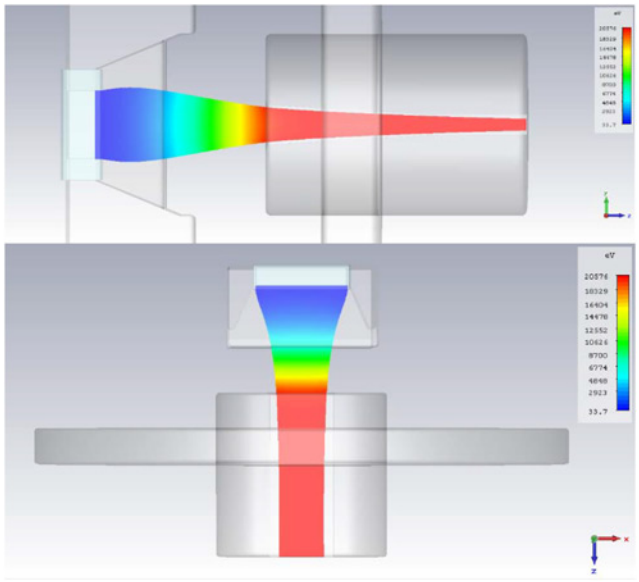

Fig. 11 *Trajectory of sheet electron beam in the electron gun*

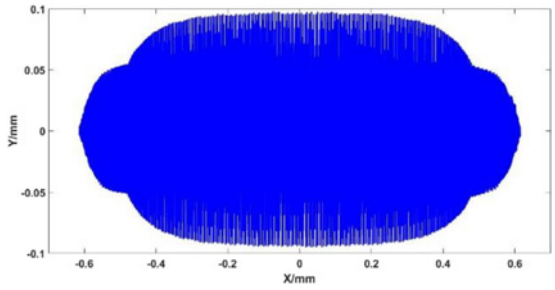

Fig. 12 *Schematic diagram of crossing section of sheet electron beam at the exit of anode channel*

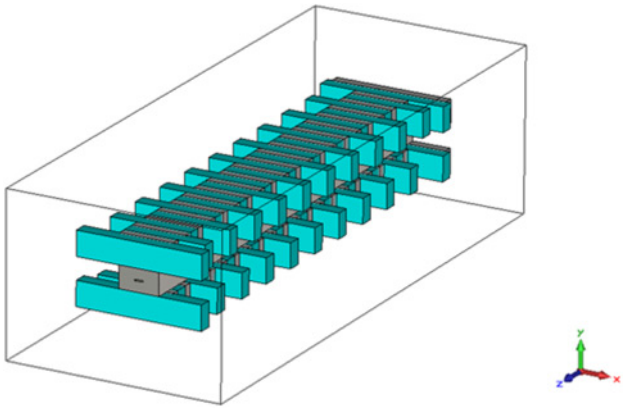

Fig. 13 *Schematic diagram of PCM focusing system*

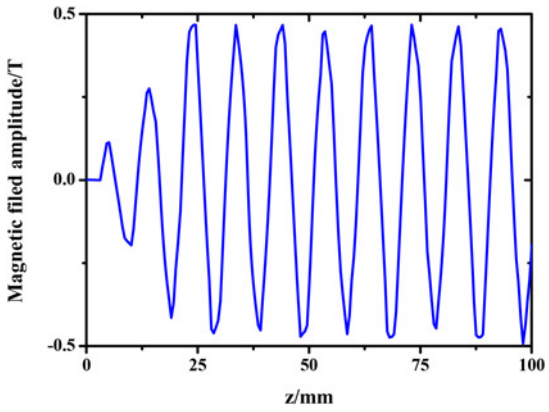

Fig. 14 *z-component magnetic field amplitude along z direction*

To focus the sheet electron beam, a y-component of the magnetic field is necessary (the narrow side of the beam tunnel is along the y direction) [18–20]. As shown in Fig. 15, the y-component magnetic field is symmetry along the x-axis and the peak amplitude approaches 0.06 T.

The propagation ratio is simulated. When the electron beam operates under voltage of 20.6 kV and current of 0.8 A, the propagation ratio is 100%. Fig. 16 shows the x–z cross section of the electron beam in the PCM focusing system, and Fig. 17 shows the y–z cross section of the electron beam in the PCM focusing system.

4. Beam–wave interaction

Taking advantage of the results discussed above, the beam–wave interaction is simulated by CST Particle Studio. The particle-in-cell solver is used. The operation voltage is 20.6 kV, current is 80 mA,

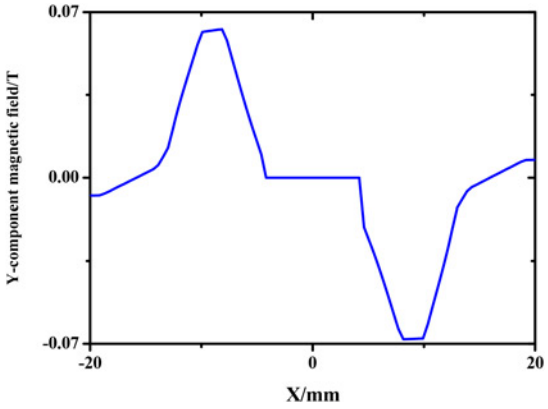

Fig. 15 *y-component magnetic field amplitude along x direction*

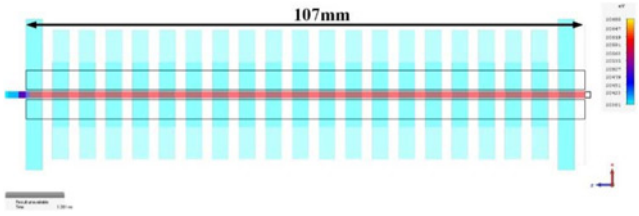

Fig. 16 *x–z cross section of beam in the PCM focusing system*

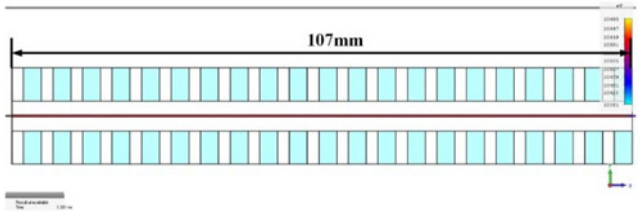

Fig. 17 *y–z cross section of beam in the PCM focusing system*

the power of input signal is 10 W, the period number before the attenuator is 25 and the period number after the attenuator is 46. As shown in Fig. 18, the amplitude of the output signal is 16 V, the output power is 126 W and the gain is 11 dB.

To increase the output power, a phase velocity taper is designed. We reset the period number so that there are 28 periods before

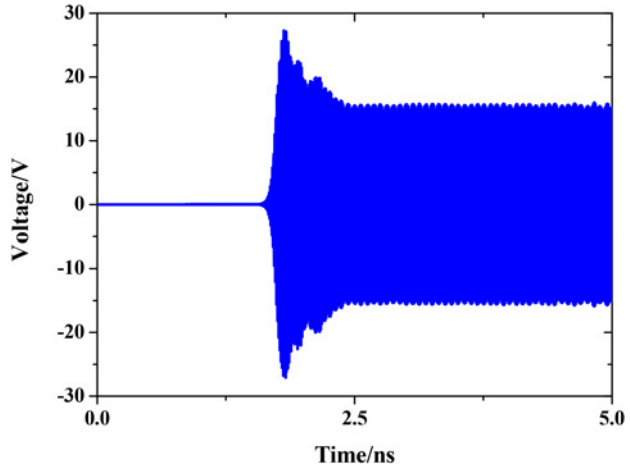

Fig. 18 *Output power without phase velocity taper*

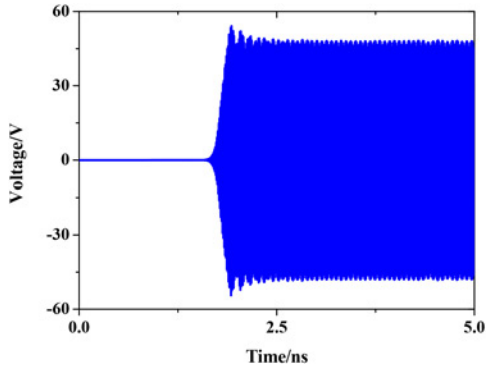

Fig. 19 *Output power with phase velocity taper*

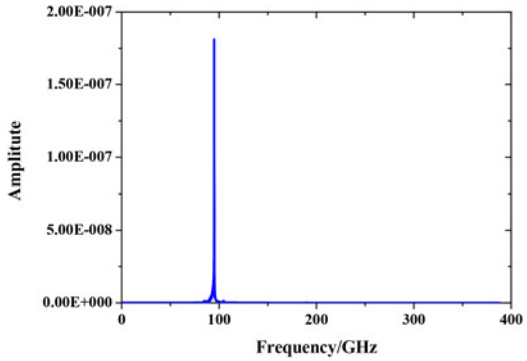

Fig. 20 *Frequency spectrum of output signal with phase velocity taper*

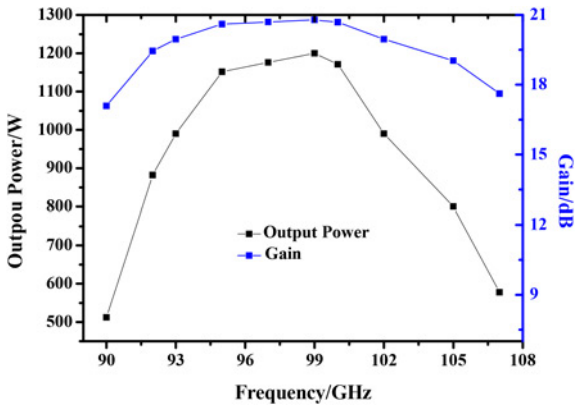

Fig. 21 *Output power and gain versus frequency*

attenuator, and the velocity taper takes place in the 18th period after the attenuator. After the 18th period, the length of the period is 1 versus 1.066 mm before. The operation voltage, current and input signal power did not change. As shown in Fig. 19, the amplitude of the output signal is 47 V, the output power is around 1100 W and the gain is 20.41 dB. Fig. 20 shows the frequency spectrum of the output signal. There is a pure signal at 95 GHz.

Fig. 21 shows the output power and the gain versus frequency from 90 to 107 GHz. The peak power is 1200 W at 99 GHz.

5. Conclusion

A W-band sheet beam TWT based on the staggered double vane SWS is designed in this study. The dispersion characteristic is simulated in section 2. Based on the dispersion curve, the operation voltage is set at 20.6 kV. An attenuator is also taken into account.

According to the analysis of transportation characteristics, the parameter S_{21} reduces from near to 0 dB to lower than −10 dB because of the attenuator that shows great effect on the attenuator. A vacuum window is designed. The material of the vacuum window is diamond. The reflection of the vacuum window is lower than −20 dB from 91 to 107 GHz.

A sheet electron beam gun supporting the W-band staggered double vane TWT is designed in section 3. A pierce electrode is utilised to focus the narrow side of the sheet electron beam. The current produced by the sheet electron beam gun is 0.814 A that also suit the demand of the high-frequency system. Plans of the PCM focusing system is also presented. The PCM focusing system could focus well on the sheet beam. The propagation ratio of the sheet electron beam is 100%.

Beam–wave interaction is simulated in section 5. To increase the output power, a phase velocity taper is used in this design. With the phase velocity taper, the output power approaches 1100 W at 95 GHz, while the gain is 20.41 dB. The peak amplitude of the output power is 1200 W at 99 GHz, while the gain is 20.79 dB.

6 Acknowledgments

This work was supported by the National Science Foundation of China (grant no. 61531010).

7 References

[1] Shin Y. M., Baig A., Barnett L. R., *ET AL.*: 'Modeling investigation of an ultrawideband Terahertz sheet beam traveling-wave tube amplifier circuit', *IEEE Trans. Electron. Devices*, 2011, **58**, (9), pp. 3213–3218

[2] He J., Wei Y., Gong Y., *ET AL.*: 'Linear analysis of a W band grooved loaded folded waveguide traveling wave tube', *Phys. Plasmas*, 2010, **17**, (11), pp. 113–305

[3] Xing S.: 'Application and development of millimetre-wave radars', *Telecommun. Eng.*, 2006, **2006**, (1), pp. 1–9

[4] Lai J., Gong Y., Xu X., *ET AL.*: 'W-band 1-kW staggered double-vane traveling-wave tube', *IEEE Trans. Electron. Devices*, 2012, **59**, (2), pp. 496–503

[5] Shin Y. M., Barnett L. R., Luhmann N. C.: 'Phase-shifted traveling-wave-tube circuit for ultrawideband high-power submillimeter-wave generation', *IEEE Trans. Electron. Devices*, 2009, **56**, (5), pp. 706–712

[6] Qiu J. X., Levush B., Pasour J., *ET AL.*: 'Vacuum tube amplifiers', *IEEE Microw. Mag.*, 2009, **10**, (7), pp. 38–51

[7] Grede A., Henke H., Sharma R. K.: 'RF-structure design for the W-band folded waveguide TWT project of CEERI'. 2011 IEEE Int. Vacuum Electronics Conf., IVEC-2011, 2011, pp. 213–214

[8] Buneman O.: 'Relativistic space-charge flow', *J. Electron. Control*, 1957, **3**, (5), pp. 509–511

[9] Cun R., Shu W., Ding Z. H. A. O., *ET AL.*: 'The development of millimeter wave sheet beam devices', *Vacuun Electron.*, 2010, **2**, pp. 8–16

[10] Carlsten B. E., Russell S. J., Earley L. M., *ET AL.*: 'Technology development for a mm-wave sheet-beam traveling-wave tube', *IEEE Trans. Plasma Sci.*, 2005, **33**, (1 I), pp. 85–93

[11] Shi X., Wang Z., Zhang Y., *ET AL.*: 'An arbitrary staggered multi-vane traveling wave tube driven by double sheet electron beams'. 2015 8th UK, Europe, China Millimeter Waves and THz Technology Workshop, UCMMT 2015, 2016, pp. 1–3

[12] Shi X., Wang Z., Tang X., *ET AL.*: 'Study on wideband sheet beam traveling wave tube based on staggered double vane slow wave structure', *IEEE Trans. Plasma Sci.*, 2014, **42**, (12), pp. 3996–4003

[13] Calame J. P., Garven M., Lobas D., *ET AL.*: 'Broadband microwave and W-band characterization of BeO-SiC and AlN-based lossy dielectric composites for vacuum electronics'. 2006 IEEE Int. Vacuum Electronics Conf. held Jointly with 2006 IEEE Int. Vacuum Electron Sources, 2006, pp. 37–38

[14] Xu L., Wang H., Li J., *ET AL.*: 'Windows simulator: an advanced three-dimensional finite-element S-parameter-simulation tool for microwave tubes'. Proc. 2015 IEEE Int. Vacuum Electronics Conf., IVEC 2015, 2015, pp. 1–2

[15] Lai J., Gong Y., Wei Y., *ET AL.*: 'An electron optical system for sheet beam vacuum electron devices'. Microwave Conf. Proc. (CJMW), 2011 China–Japan Joint, 2011, pp. 22–24

[16] Tang X.-F., Duan Z.-Y., Wang Z.-L., *ET AL.*: 'The design method of millimeter-wave sheet-beam electron gun', *J. Infrared Millim. Waves*, 2014, **33**, (6), pp. 619–624

[17] Booske J. H., Basten M. A.: 'Demonstration via simulation of stable confinement of sheet electron beams using periodic magnetic focusing', *IEEE Trans. Plasma Sci.*, 1999, **27**, (1), pp. 134–135

[18] Booske J. H., Basten M. A., Kumbasar A. H., *ET AL.*: 'Periodic magnetic focusing of sheet electron beams', *Phys. Plasmas*, 1994, **1**, (5), pp. 1714–1720

[19] Booske J. H., McVey B. D., Antonsen T. M.: 'Stability and confinement of nonrelativistic sheet electron beams with periodic cusped magnetic focusing', *J. Appl. Phys.*, 1993, **73**, (9), pp. 4140–4155

[20] Zhao D., Lu X., Liang Y., *ET AL.*: 'Researches on an X-band sheet beam klystron', *IEEE Trans. Electron Devices*, 2014, **61**, (1), pp. 151–158